ACS APPLIED MATERIALS & INTERFACES

Research Article

www.acsami.org

Highly Sensitive Electrochemical Biosensor for Evaluation of Oxidative Stress Based on the Nanointerface of Graphene Nanocomposites Blended with Gold, Fe_3O_4, and Platinum Nanoparticles

Le Wang, Yuanyuan Zhang, Chuansheng Cheng, Xiaoli Liu, Hui Jiang, and Xuemei Wang*

State Key Laboratory of Bioelectronics, School of Biological Science and Medical Engineering, Southeast University, Nanjing 210096, China

Supporting Information

ABSTRACT: High levels of H_2O_2 pertain to high oxidative stress and are associated with cancer, autoimmune, and neurodegenerative disease, and other related diseases. In this study, a sensitive H_2O_2 biosensor for evaluation of oxidative stress was fabricated on the basis of the reduced graphene oxide (RGO) nanocomposites decorated with Au, Fe_3O_4, and Pt nanoparticles (RGO/$AuFe_3O_4$/Pt) modified glassy carbon electrode (GCE) and used to detect the released H_2O_2 from cancer cells and assess the oxidative stress elicited from H_2O_2 in living cells. Electrochemical behavior of RGO/$AuFe_3O_4$/Pt nanocomposites exhibits excellent catalytic activity toward the relevant reduction with high selection and sensitivity, low overpotential of 0 V, low detection limit of ~0.1 μM, large linear range from 0.5 μM to 11.5 mM, and outstanding reproducibility. The as-prepared biosensor was applied in the measurement of efflux of H_2O_2 from living cells including healthy normal cells and tumor cells under the external stimulation. The results display that this new nanocomposites-based biosensor is a promising candidate of nonenzymatic H_2O_2 sensor which has the possibility of application in clinical diagnostics to assess oxidative stress of different kinds of living cells.

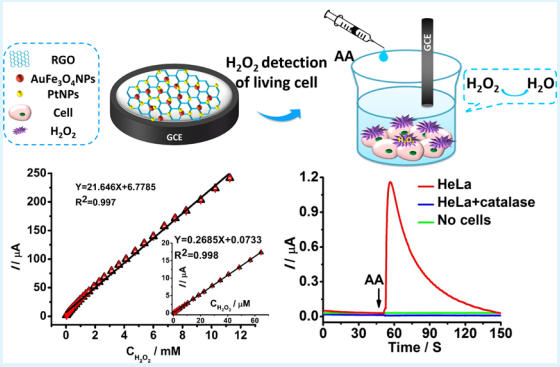

KEYWORDS: *hydrogen peroxide, graphene nanosheets, gold nanoparticles, ferroferric oxide nanoparticles, Pt nanoparticles, electrochemical detection, living cell*

1. INTRODUCTION

Reactive oxygen species (ROS) are considered as the significant intracellular signaling molecules which can regulate DNA damage, protein synthesis, cell apoptosis, and other living activities, which exist in the aerobic organisms during their whole life.[1−3] It is already known that ROS could be endowed *in vivo* with several physiology functions such as immunity activity and signal transition process. However, an excess of ROS accumulation in cells gives rise to internal sabotage activity and leads to oxidative stress which was recognized as the root of caducity and diseases, resulting in destroying the balance of organic redox reaction and biological normal cells and tissues and causing a variety of pathological events such as neurodegeneration, Alzheimer's disease, autoimmune diseases, and cancer.[4−6] Hydrogen peroxide (H_2O_2) is one of the major representatives of oxidative stress damage due to its long lifetime in which it can penetrate into other cellular compartments and become distributed in most of the mammalian cells. Therefore, the selective and accurate measure of H_2O_2 in cells and the dynamic observation of living cells are important to illuminate the mechanism of regulating signal transduction pathways and further exploit the potential application in clinical pathological diagnosis.[7] Therefore, various kinds of H_2O_2 detection methods have been employed such as florescence,[8] chemiluminescence,[9] chromatography,[10] and electrochemical analysis.[11,12] Among them, electrochemical technology is considered as one of the most promising strategies on account of its high sensitivity, fast response, production simplicity, low cost, and low detection limit.[13] In the past several years, enzyme-based electrochemical biosensors have always been the research highlights, which are immobilized with enzymes in the functionalized electrodes, such as horseradish peroxidase,[14] glucose oxidase,[15] cytochrome,[16] and myoglobin.[17] In spite of the high sensitivity and good selectivity in the moderate condition, the application prospects of enzyme-based sensors are restricted by the inevitable disadvantages such as high costs, a complicated immobilization procedure,[18] the influenced instability, and reproduction caused by environment.[19] In comparison with enzymatic sensor, nonenzymatic sensors based on nanomateri-

Received: May 25, 2015
Accepted: August 4, 2015
Published: August 4, 2015

DOI: 10.1021/acsami.5b04553
ACS Appl. Mater. Interfaces 2015, 7, 18441−18449

Scheme 1. Schematic of the RGO/$AuFe_3O_4$/Pt-Modified GCE Used for Detecting H_2O_2 Efflux from Cells Stimulated with AA

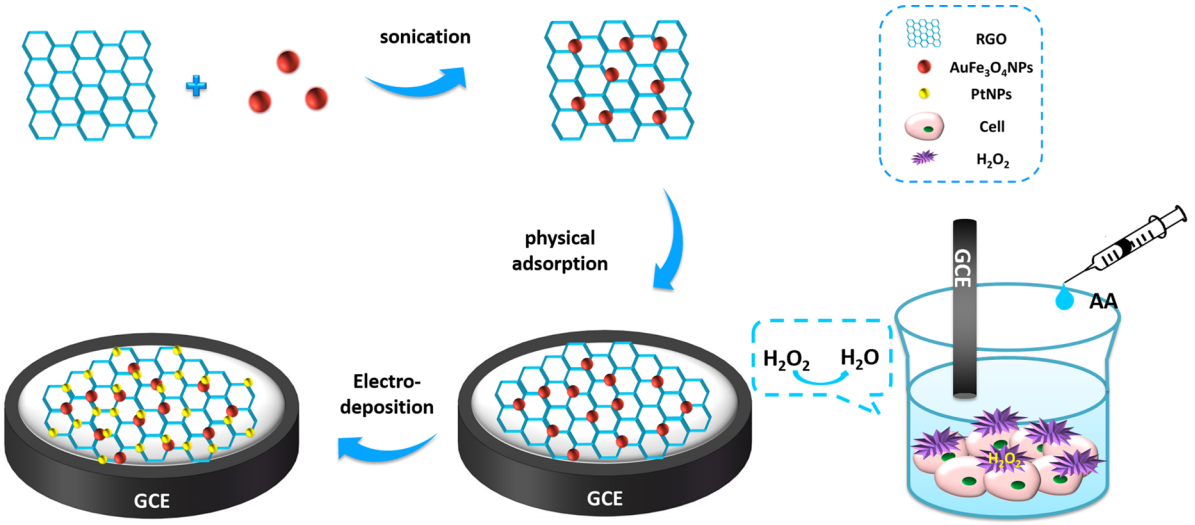

als reveal many advantages such as high electrocatalytic activity, specific surface area, and outstanding electron transfer ability. Therefore, we hypothesized to fabricate a highly sensitive nonenzymatic H_2O_2 biosensor to detect the H_2O_2 concentrations released from different kinds of cells stimulated by extracellular matters and further to evaluate the oxidative stress of different living cells.

Graphene has attracted tremendous attention resulted from the outstanding properties such as high surface area, superior electric conductivity, good mechanical strength, and so on.[20,21] Especially, reduced graphene oxide (RGO) composited through the reduction of graphene oxide owns several functional groups such as hydroxyl (-OH) and carboxyl (-COOH) groups resulting in the higher conductivity, which is favored for nucleation and growth of metal nanoparticles in the fabrication of nanocomposites.[22,23] Graphene is widely used in electrochemical catalysis of H_2O_2; however, the liner range and sensitivity are not enough for H_2O_2 detection in living cells.[24,25] The combination of graphene and metal nanoparticles usually lead to larger electrochemically active surface areas and higher electron transfer rate to improve the current response more sensitively.[26,27] Au nanoparticles possess rapid electron transfer, efficient electrocatalytic properties, and good biocompatibility,[20,21] particularly when dispersed on an oxide support often with much better performance in catalytic activity than the single-component nanoparticles,[28−30] due to the synergetic effect at the interface of metal and oxide support which can also provide more active sites.[31,32] In spite of the observation that the dumbbell-like $AuFe_3O_4$ nanoparticles display catalytic activity for H_2O_2 reduction,[31] there is very limited study on the application of $AuFe_3O_4$ nanoparticles in the area of highly sensitive biosensor and evaluation of oxidative stress. In addition, Pt nanoparticles possess good stability, high electrocatalytic efficiency, and good selectivity and have been extensively utilized as the electrochemical electrode material for construction of biosensor.[33,34] What's more important is that Pt nanoparticles can readily reduce the H_2O_2oxidation−reduction overvoltage.[34] In view of the preceding considerations, the integration of graphene, $AuFe_3O_4$ nanoparticles, and Pt nanoparticles are supposed to employ characteristic performance in the application of catalysis, electrons, and biosensor, and overcome the existing limitations, resulting from the synergistic effect of each composition.

Herein, in this study a novel RGO/$AuFe_3O_4$/Pt nanocomposition based on nonenzymatic H_2O_2 sensor was fabricated and utilized to detect the H_2O_2 released from living cells (Scheme 1). The blending of the nanosheets of reduced graphene oxide with Au Fe_3O_4 nanoparticles ($AuFe_3O_4$ NPs) and Pt nanoparticles (Pt NPs) were modified on a glassy carbon electrode (GCE) through physical adsorption and electrodeposition. The as-prepared RGO/$AuFe_3O_4$/Pt nanocomposites modified GCE (i.e., RGO/$AuFe_3O_4$/Pt-GCE) reveals much higher current response on the H_2O_2 reduction process compared with the RGO/$AuFe_3O_4$NPs and Pt NPs modified GCE, exhibiting the high sensitivity, the fast response time, large linear range, and low detection limit in the measurement of H_2O_2. This novel nonenzymatic H_2O_2 biosensor can be readily employed to detect the H_2O_2 released from the living cells during the redox homeostasis disrupted by ascorbic acid and to further evaluate the intracellular H_2O_2 concentration, indicating that the oxidative stress level in the tumor cells is much higher than that of normal cells, which has significance in the application of acquainting the information on the intracellular environment in the tumor developing process.

2. EXPERIMENTAL SECTION

2.1. Reagents and Apparatus. Reduced graphene oxide was purchased from XF NANO, Inc. (China). Chloroplatinic acid ($H_2PtCl_6{\cdot}6H_2O$) was purchased from Sigma-Aldrich and was used as received. Ascorbic acid (AA), β-D(+)-glucose, uric acid (UA), and chitosan (CHIT) were obtained from Sigma. H_2O_2 was obtained from International Laboratory. All other chemicals were of reagent grade and were used as received without any further purification.

A 0.02 M phosphate buffer solution (PBS, pH 7.4) consisting of NaH_2PO_4 and Na_2HPO_4 was used as the supporting electrolyte. A physiological PBS solution containing KH_2PO_4 (1.76 mM), Na_2HPO_4 (10.14 mM), NaCl (136.75 mM), and KCl (2.28 mM), was mainly used for washing of living cells and observing the H_2O_2 released from the cells. All of the solutions were prepared with doubly distilled water.

The morphologies and surface structures were characterized with a scanning electron microscope (SEM; Zeiss, Germany). The valence states of the relevant nanocomposites were investigated by a PHI Quantera II X-ray photoelectron spectrometer (XPS). All electrochemical measurements were performed on a CHI660B electrochemical workstation (CHI Inc., USA). A conventional three-electrode

DOI: 10.1021/acsami.5b04553
ACS Appl. Mater. Interfaces 2015, 7, 18441−18449

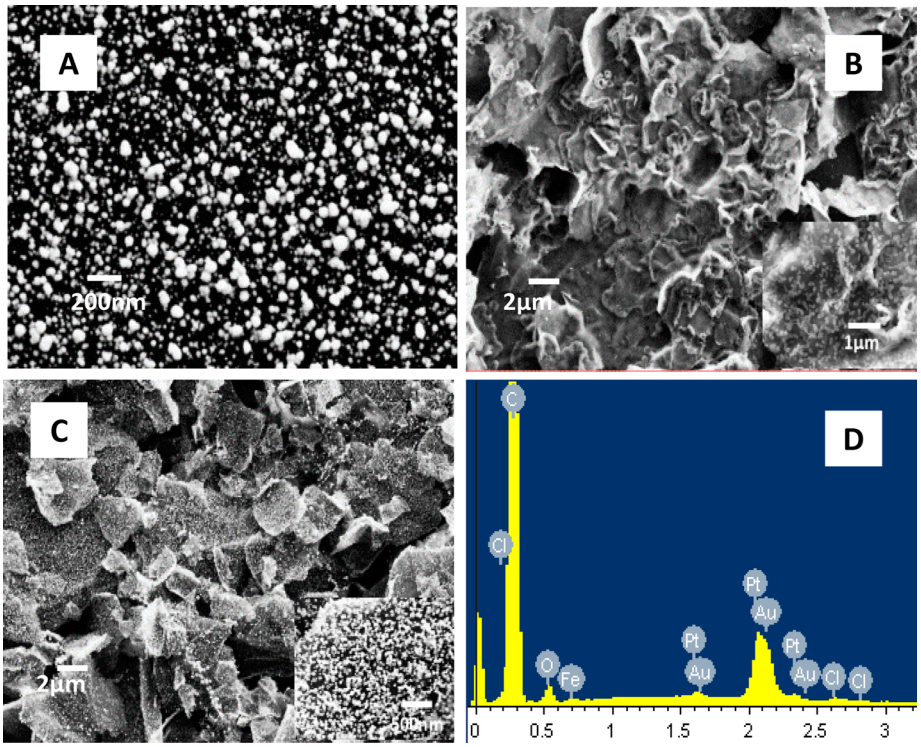

Figure 1. SEM images of Pt NPs (A), RGO/$AuFe_3O_4$ NPs (B), and RGO/$AuFe_3O_4$/Pt NPs (C) on GCE. Panel D is the EDS of RGO/$AuFe_3O_4$/Pt nanocomposites.

system employing a bare or modified glassy carbon working electrode, an AglAgCl reference electrode, and a platinum wire counter electrode was used. All potentials were measured and reported versus the Agl AgCl reference electrode. All amperometric measurements were regularly accomplished in 0.02 M PBS (pH 7.4) with stirring. The electrolyte was ventilated with high-purity nitrogen for 20 min, and then the electrochemical measurements were performed inside the deoxygenated atmosphere during experiments.

2.2. Preparation of RGO/$AuFe_3O_4$NPs Composite Materials. A 0.032 g amount of NaOH was added into 15 mL of DEG and dissolved in an ultrasonic bath for 30 min and then added with 1 mL of DEA. A 0.0541 g amount of $FeCl_3$, 0.0199 g of $FeCl_2$, and 15 mL of DEG were added to the three-necked flask and heated to 80 °C in the flow of N_2.The as-prepared DEG with NaOH was added into the three-necked flask to react for 1 h, and then 1 mL of $HAuCl_4$ (0.01 M) was added into the hybrid. The prepared reaction products were put into the reaction still and heated on 200 °C for 8 h before being cooled to room temperature. The obtained solution was isolated in a centrifugal machine at a rate of 9000 rpm for 10 min and then washed thoroughly and dispersed with twice-distilled water and alcohol for 3 times. Eventually, the $AuFe_3O_4$ NPs were composed after the processes discussed previously.

RGO suspension was dispersed in doubly distilled water under sonication for 2 h. A 0.2 mL aliquot of RGO solution (2 mg/mL) was mixed with 0.2 mL of $AuFe_3O_4$ solution (0.5 mM) and 0.6 mL of CHIT solution (1 mg/mL) and then was stirred for 20 min to obtain the RGO/$AuFe_3O_4$ NPs composite. RGO/$AuFe_3O_4$NPs composite was dispersed by ultrasonication to acquire a suspension before use.

2.3. Preparation of the Modified Electrodes. Glassy carbon electrode (GCE, 3 mm in diameter) was carefully polished with 0.3 and 0.05 μm alumina slurry on a microcloth (Buehler, USA), cleaned by ultrasonication in ethanol, and deionized water for 3 min. A certain volume of RGO suspension was cast onto the surface of GCE as working electrode and allowed to dry in air for 3 h at room temperature; the optimal volume is reported later. The Pt NPs were deposited in 2 mM H_2PtCl_6 solution by cyclic voltammetry (CV) in the range between −1 V and +1 V with a scan rate of 50 mV/s. The modified electrode was cleaned carefully by doubly distilled water in order to remove the remaining H_2PtCl_6 and dried at room temperature. The supporting electrolyte of PBS (0.02 M, pH 7.4) containing NaH_2PO_4 and Na_2HPO_4 was deoxygenated using nitrogen and kept inside a nitrogen atmosphere.

2.4. Cell Culture. HeLa (human cervical cancer cell lines), U87 (human primary glioblastoma cell lines), and HepG2 (human hepatocarcinoma lines) cells were bought from the Institute of Hematology, Chinese Academy of Medical Sciences. L02 (human embryo liver cell lines) cells were obtained from the Third Military Medical University (Chongqing, China). They were cultivated at 37 °C with 5% CO_2 in a 95% humid atmosphere with DMEM (high glucose, Gibco) containing 10% heat-inactivated fetal calf serum (Sigma-Aldrich, St. Louis, MO, USA), 100 U/mL penicillin (Sigma-Aldrich), and 100 mg/mL streptomycin (Sigma-Aldrich).

2.5. Electrochemical Detection of H_2O_2 Released by Cells. Cell number was calculated by using a cell counter. Cells were divided from the culture medium through centrifugation for 4 min at 1500 rpm and washed three times by the physiological PBS (0.02 M, pH 7.4) solution. Ascorbic acid (AA) was injected into cells as the stimulation to motivate cells to generate H_2O_2 after the current was reduced to less than 20 nA. The detection of H_2O_2 was not interrupted with the addition of AA. The amperometric current response of H_2O_2 released from approximately 5.0×10^6 cells was measured by RGO/$AuFe_3O_4$/Pt-modified GCE at 0 V in 1 mL of deoxygenated PBS.

3. RESULTS AND DISCUSSION

3.1. Characterization of RGO/$AuFe_3O_4$ and Pt NPs on Electrode Surface. The SEM images shown in Figure 1 exhibit the general morphology of electrodes modified with different nanomaterials (i.e., Pt, RGO/$AuFe_3O_4$, and RGO/$AuFe_3O_4$/Pt) employed in this research. Figure 1A displays the external surface of RGO/$AuFe_3O_4$ modified on the GCE, showing the structure of wrinkled multilayer stacks with small sticking $AuFe_3O_4$ nanoparticles. Figure 1B reveals the electrodeposited Pt NPs with the size of 50 nm. It can be seen from

DOI: 10.1021/acsami.5b04553
ACS Appl. Mater. Interfaces 2015, 7, 18441−18449

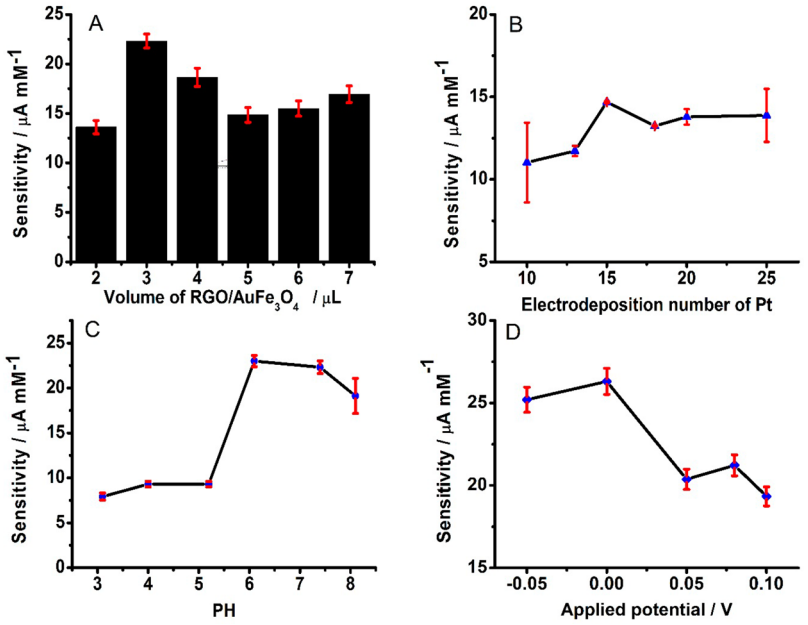

Figure 2. Optimization study of $RGO/AuFe_3O_4$ NPs volume deposited on the GCE (A), the CV cycles for electrochemical deposition of Pt NPs on the $RGO/AuFe_3O_4$-GCE (B), the pH value of PBS solution (C), and the applied potential employed (D). Error bars are the standard error of the mean (n = 4 electrodes).

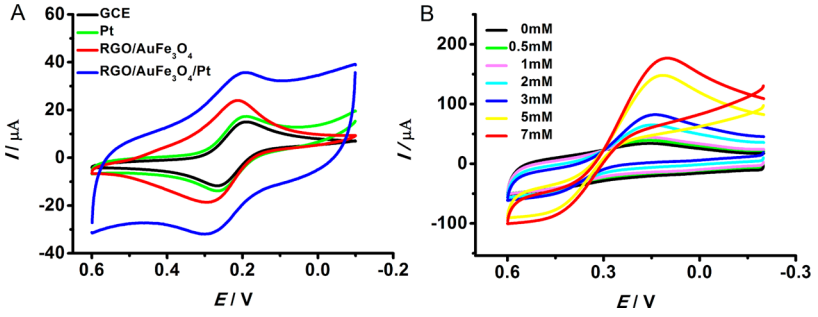

Figure 3. (A) CVs of bare, Pt, $RGO/AuFe_3O_4$, and $RGO/AuFe_3O_4/Pt$ modified GCEs in potassium ferricyanide solution containing 0.1 M KCl and 1 mM $K_3[Fe(CN)_6]$. (B) CVs of $RGO/AuFe_3O_4/Pt$-GCE in the absence and presence of different concentrations of H_2O_2 in 0.02 M PBS. Scan rate: 100 mV/s.

Figure 1C that a large amount of well-distributed Pt NPs electrodeposited densely on the $RGO/AuFe_3O_4$ surface, composing the $RGO/AuFe_3O_4/Pt$ nanocomposites. From Figure 1D, it can be obtained that the EDS result demonstrates the primary composites of $RGO/AuFe_3O_4/Pt$ nanocomposites including C, Pt, Au, and Fe elements. Meanwhile, as shown in Figure S1 to Figure S3 of the Supporting Information, the XPS studies of relevant nanocomposites of the modified electrode also confirm the corresponding components of the as-prepared nanostructural modification.

3.2. Optimization Study of $RGO/AuFe_3O_4/Pt$ Nanocomposites Modified Electrodes. As shown in Figure 2, the deposition parameters of nanomaterials and pH value have a significant impact on the sensitivity of H_2O_2 detection. Figure 2A shows that adding volume of deposited $RGO/AuFe_3O_4$ leads to the increasing detection sensitivity of H_2O_2, reaching a peak value at the volume of 3 μL.Then the sensitivity declined with the addition of deposition volume and attained a minimum value at 6 μL. Afterward, the increasing deposition of $RGO/AuFe_3O_4$ enhanced the H_2O_2 detection sensibility. From Figure 2B, it is noted that the sensitivity response to H_2O_2 detection has a maximum when the deposition CV cycles of Pt NPs was 15. Meanwhile, the influence of different pH values of PBS solution on H_2O_2 detection was researched. As shown in Figure 2C, in the range of pH 3.0−8.0, the sensitivity of H_2O_2 detection was relatively low in the acidic environment and reached a peak at pH 7.4. The applied potential usually has a large effect on the sensitivity. It can be seen from Figure 2D that, in the range from −0.05 to 0.1 V, the sensitivity increased with the increase of potential, reached the maximum at 0 V, and then decreased with the further rise of the applied potential. To avoid the interference of other substances under high negative potential, 0 V was selected in experiments. Therefore, 3 μL of $RGO/AuFe_3O_4$, 15 CV cycles for Pt NPs deposition, PBS solution of pH 7.4 and applied potential of 0 V were employed in this study.

3.3. Electrocatalytic Reduction of H_2O_2 on $RGO/AuFe_3O_4/Pt$ Nanocomposites Modified Electrode. To investigate the electrocatalytic activity of the nanointerface of $RGO/AuFe_3O_4/Pt$ nanocomposites for a nonenzymatic H_2O_2 sensor, cyclic voltammetry was employed in a range from −0.1 V to +0.6 V at a scan rate of 0.1 V/s in pH 7.4 PBS on $RGO/AuFe_3O_4/Pt$ nanocomposites modified glassy carbon electrode ($RGO/AuFe_3O_4/Pt$-GCE). In this work, CV was employed to

DOI: 10.1021/acsami.5b04553
ACS Appl. Mater. Interfaces 2015, 7, 18441−18449

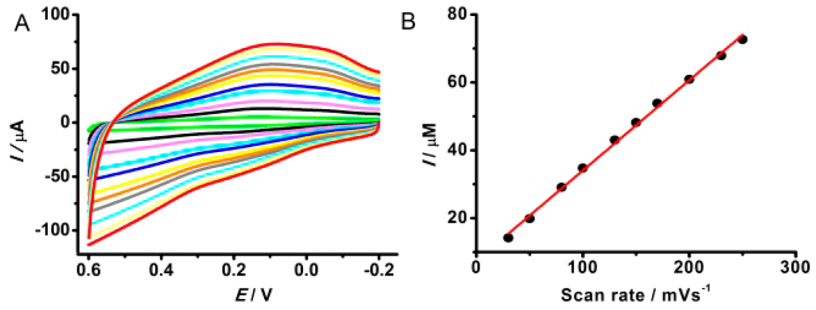

Figure 4. (A) CVs of RGO/$AuFe_3O_4$/Pt-GCE in 0.02 M PBS at a scan rate of (from inner to outer): 30, 50, 80, 100, 130, 150, 170, 200, 230, and 250 mV/s, respectively. (B) Linear relationship between the peak currents and the scan rates.

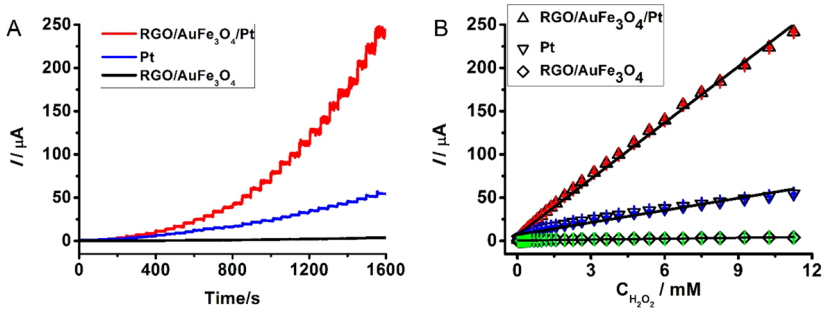

Figure 5. (A) Amperometric response of RGO/$AuFe_3O_4$/Pt-GCE, Pt-GCE, and RGO/$AuFe_3O_4$-GCE to successive additions of H_2O_2 at 0 V in 0.02 M PBS. (B) Linear relation between the amperometric response and H_2O_2 concentration. Error bars are the standard error of the mean (n = 4 electrodes).

quantify the relevant electrochemical parameters and measured in the electrolyte solution consisting of 1 mM $K_3[Fe(CN)_6]$ and 0.1 M KCl. It can be seen from Figure 3A that a pair of well-defined redox peaks was observed as the result of the $[Fe(CN)_6]^{3-/4-}$ oxidation−reduction couples. The electroactive surface area of electrodes was calculated on the basis of the Randled−Sevcik equation. At the temperature of 25 °C, the Randled−Sevcik equation is expressed as $I_p = 2.69 \times 10^5 AD^{1/2}n^{3/2}\gamma^{1/2}C$, where I_p means the peak current (A); A means the effective surface area of electrode (cm^2); D means the diffusion coefficient of the reagent, which is $(6.7 \pm 0.02) \times 10^{-6}$ cm^2 s^{-1} for $K_3[Fe(CN)_6]$; n means the number of transition electrons in the oxidation−reduction reaction, which is 1 for $[Fe(CN)_6]^{3-/4-}$; γ means the scan rate (V s^{-1}); and C is the concentration of the redox reactant (mol cm^{-3}). The calculated electroactive surface areas of electrodes were in the tendency of bare GCE (0.06736 cm^2) < Pt-GCE (0.07879 cm^2) < RGO/$AuFe_3O_4$-GCE (0.10823 cm^2) < RGO/$AuFe_3O_4$/Pt-GCE (0.14265 cm^2), revealing that the three-dimensional skeleton, good electrical conductivity of RGO/$AuFe_3O_4$, and well-distributed Pt NPs on the GCE surface can bring about the enlarged electroactive surface area.

The admirable three-dimensional structure and uniformly distributed nanomaterials lead to the excellent performance of the molecules transfer and electron conductivity of RGO/$AuFe_3O_4$/Pt nanocomposites. Therefore, there is significance to research of the electrocatalytic activity of H_2O_2 electroreduction on the RGO/$AuFe_3O_4$/Pt nanocomposites modified electrode interface. Figure 3B displays the CV curves of RGO/$AuFe_3O_4$/Pt nanocomposites modified GCE in 0.02 M PBS solution (pH 7.4) in the absence and presence of H_2O_2 of different concentrations. As exhibited in Figure 3B, an obvious reduction peak around 0.15 V emerges in the presence of 0.5 mM H_2O_2. As the concentration of H_2O_2 increases, the reduction current is dramatically enhanced, accompanied by the reduction peak which becomes sharp and shifts to negative potential slightly, presumably as the result of the torpid electron transfer kinetics. The obvious reduction current displays that H_2O_2 can be easily reduced on RGO/$AuFe_3O_4$/Pt nanostructures in a large concentration range. The outstanding electrocatalytic activity of RGO/$AuFe_3O_4$/Pt-GCE benefits from the characteristic three-dimensional nanostructures, high surface-to-volume ratio, and the collaborative contributions afforded by RGO/$AuFe_3O_4$ and Pt nanoparticles. It implies that RGO/$AuFe_3O_4$/Pt nanocomposites have great application potential in H_2O_2 biosensing.

3.4. Electrochemical Properties of RGO/$AuFe_3O_4$/Pt Nanocomposites Modified GCE. The CV technology was measured to investigate the charge transport characteristics of the RGO/$AuFe_3O_4$/Pt nanocomposite film at different scan rates between −0.2 and 0.6 V vs AglAgCl. It is shown in Figure 4A that the slight peak potential changes from 0.12 to 0.09 V when the scan rate reaches 100 mV/s and then remains at 0.09 V stably with the increase in scan rate. The negative shift of the related reduction peak potential may be caused by the sluggish electron transfer kinetics.[4] Meanwhile, the anodic and cathodic peak currents increased with the increase of scan rates from 30 to 250 mV/s, with a correlation coefficient of 0.996 as exhibited in Figure 4B, which demonstrates that the redox process of RGO/$AuFe_3O_4$/Pt modified electrode surface is a surface-confined process with the quick electron transfer kinetics. It can be obtained that the $AuFe_3O_4$/Pt composition was dispersed on the surface of RGO and personality of nice conductivity of the RGO/$AuFe_3O_4$/Pt nanomaterial.

3.5. Amperometric Response to H_2O_2 Detection. Figure 5A displays the amperometric response of the RGO/$AuFe_3O_4$/Pt-modified electrode to the successive addition of varying concentrations in 0.2 M pH 7.4 PBS solution and the

DOI: 10.1021/acsami.5b04553
ACS Appl. Mater. Interfaces 2015, 7, 18441−18449

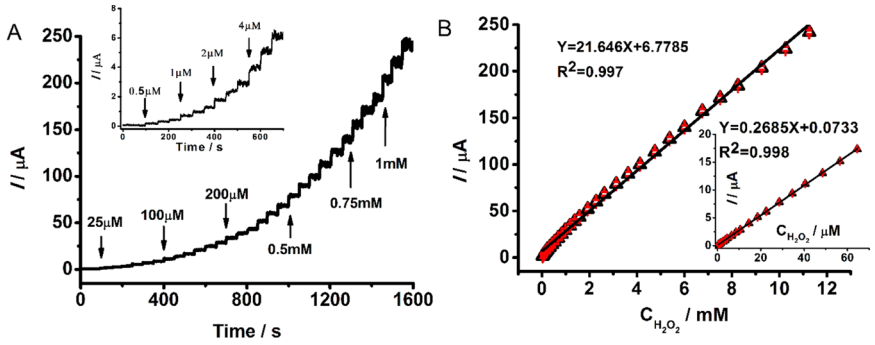

Figure 6. (A) Amperometric response of RGO/$AuFe_3O_4$/Pt-GCE to successive additions of H_2O_2 at 0 V in 0.02 M PBS (H_2O_2 was added at the point indicated by arrows to the concentrations mentioned in A). (B) Linear relation between the amperometric response and H_2O_2concentration ranging from 0.025 to 11.5 mM and from 0.5 to 22.5 μM (inset B).

typical $i-t$ curves at 0 V. It can be seen that RGO/$AuFe_3O_4$/Pt-GCE proved to have an enhanced amperometric response for H_2O_2 detection compared with RGO/$AuFe_3O_4$-GCE and Pt-GCE. No obvious signal or only weak amperometric response to the addition of H_2O_2 was received on the RGO/$AuFe_3O_4$-GCE (the blue curve) and Pt-GCE (the black curve), respectively. Owing to the excellent electrocatalytic activity of RGO/$AuFe_3O_4$ nanocomposites to H_2O_2, a nonenzymatic sensor was constructed for the detection of H_2O_2. It was obtained that the sensor responded quickly to the change of H_2O_2 concentration and achieved 95% of the steady-state current within 4 s after the injection of H_2O_2 (the red curve). Figure 5B exhibits the corresponding calibration curve for the nonenzymatic H_2O_2 sensor, indicating that RGO/$AuFe_3O_4$/Pt-GCE reveals a great increased sensitivity. The RGO/$AuFe_3O_4$/Pt-modified sensor has had a linear relationship with the concentration of H_2O_2 in the range of 0.025−2 mM with a correlation coefficient of R^2 = 0.998. The linear regression equation for RGO/$AuFe_3O_4$/Pt-GCE was $I/\mu A$ = 26.31C + 1.31 (where C is the concentration of H_2O_2) with a sensitivity of 184.43 ± 5 mA M^{-1} cm^{-2} based on n = 5 electrodes. The linear regression equation for Pt-GCE was $I/\mu A$ = 4.6917C + 7.23 with a sensitivity of 59.55 ± 3 mA M^{-1} cm^{-2} based on n = 5 electrodes.

From Figure 6, there were two segments in the relevant linear range for the detection of H_2O_2 at the applied potential of 0 V, which were 0.5 × 10^{-6} to 6.45 × 10^{-4} M (correlation coefficient R^2 = 0.998) and 8.25 × 10^{-4} to 11.5 × 10^{-3} M (correlation coefficient R^2 = 0.997). The limit of detection for the H_2O_2 sensor was calculated to be ~0.1 μM (ratio of signal-to-noise (S/N) = 3). These results indicate that the excellent performance of a wide linear range, low detection potential, and high sensitivity endow RGO/$AuFe_3O_4$/Pt nanocomposites as a promising material for nonenzymatic H_2O_2 amperometric sensing.

The anti-interference ability is one of the most important analytical factors for a sensor. The influence of some electroactive species on the response of a sensor to 0.1 mM $H_2O_2$was evaluated at the potential of 0 V. A 0.1 mM amount of H_2O_2, 1.0 mM uric acid, 1.0 mM glucose, 0.5 mM AA, and a second injection of 0.1 mM H_2O_2 were added into N_2-saturated PBS to investigate the anti-interference ability of the RGO/$AuFe_3O_4$/Pt-modified nonenzymatic sensor. Figure 7 displays that there was no obvious current response after the addition of UA, AA, and GLU in the same sample. The current response to the addition of H_2O_2 was not affected in the presence of other electroactive species, indicating that UA, AA, and GLU have no

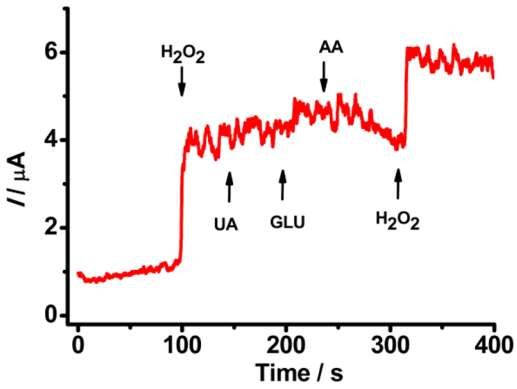

Figure 7. Amperometric response to successive addition of 0.1 mM H_2O_2, 1.0 mM UA, 1.0 mM GLU, 0.5 mM AA, and a second 0.1 mM H_2O_2 of RGO/$AuFe_3O_4$/Pt-GCE at 0 V in 0.02 M PBS.

interference in the determination of H_2O_2. The high selectivity of this sensor is primarily due to the appropriately applied potential and nanocomposites used.

The tests of reproducibility and storage stability are very important for H_2O_2 sensor. The excellent reproducibility with a relative standard deviation less than 3.94% (RSD) for the H_2O_2sensitivity was obtained on the basis of six independent RGO/$AuFe_3O_4$/Pt-GCEs. The as-prepared RGO/$AuFe_3O_4$/Pt-GCE was stored at room temperature while the sensor was out of use. The storage stability of the constructed sensor was received by measuring the current response to 0.25 mM H_2O_2 once a day. As reported in the variation of the response, sensitivity at RGO/$AuFe_3O_4$/Pt-GCE declined to about 86% of its initial response sensitivity and remained steady for 2 weeks, indicating long-term stability. All of the research data imply that the outstanding performance of the wide linear range, low detection, low detection limit, and high sensitivity can bring about the reliability of RGO/$AuFe_3O_4$/Pt-GCE in the area of H_2O_2 sensitive detection.

3.6. Measurements of H_2O_2 Release from Living Cells.

This novel nonenzymatic biosensor based on the RGO/$AuFe_3O_4$/Pt nanocomposites was explored to detect H_2O_2 in living cells. Scheme 1 shows the scheme of electrochemical detection of cellular flux of H_2O_2 under the stimulation of AA on the RGO/$AuFe_3O_4$/Pt-modified GCE. Three kinds of tumor cell lines and one kind of normal cell lines were selected as models in our study, i.e., human hepatocyte line L02, human cervical cancer cell HeLa, human hepatoma cell HepG2, and human glioma cell U87.

DOI: 10.1021/acsami.5b04553
ACS Appl. Mater. Interfaces 2015, 7, 18441−18449

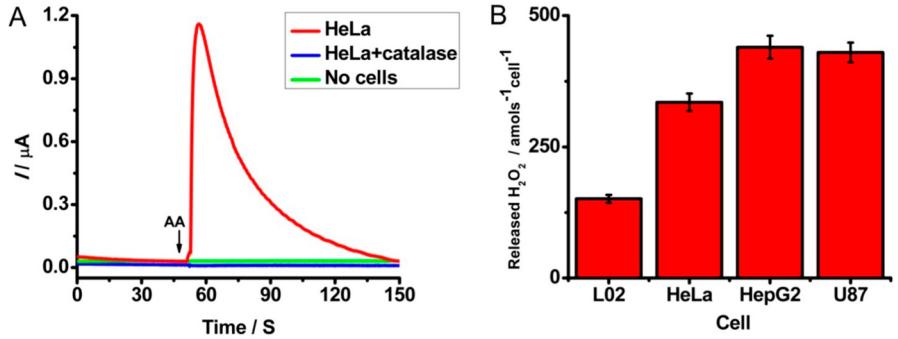

Figure 8. (A) Amperometric response upon addition of AA at 0 V in PBS containing HeLa cells (red), HeLa cells and catalases (blue), without cells (green). (B) Amount of H_2O_2 released by L02, HeLa, HepG2, and U87 cell lines stimulated by 1 μM AA. The values are expressed as means ± SD of at least three independent measurements.

Figure 8 depicts the amperometric responses obtained at the RGO/AuFe$_3$O$_4$/Pt-GCE in the presence of HeLa cells stimulated by 1 μM AA in physiological PBS buffer at 0 V versus AglAgCl. To be the control groups, the cells with catalase (blue line, Figure 8A) and the buffer solution without the cells (green line, Figure 8A) were also employed under the same conditions, and there was no current change obtained. After the addition of AA, the current caused by H_2O_2 elimination in HeLa cells was increased prominently, and the current reached a peak and then decreased to ca. 50% of the maximum in 30 s. However, the current in the control group preadded in the PBS with 500 U/mL catalase almost showed no changes (blue line, Figure 8A). The invariable current response can be resulted from the catalase introduced unique decomposition of released H_2O_2 from HeLa cells under the stimulation of AA.[2] The current change of HeLa was obtained by integration of the curve peak after AA irritation, which was about 10.86 μA, corresponding to 40.55 μM H_2O_2 in HeLa cell solution, as calculated from the standard curve displayed in the inset of Figure 8B. The volume of the cell solution was 1 mL and continuing time was 100 s, which is equivalent to 0.578 nmol of released H_2O_2. The amounts of measured HeLa cells were approximately 5.0 × 10^6, and the H_2O_2 liberated from each cell was almost 335 ± 28.5 amol. The efflux amounts of H_2O_2 from HepG2, L02, and U87 cell lines were analyzed by the same method discussed earlier. As for normal cell lines L02, the H_2O_2 amount was calculated to be ∼151 ± 20.6 amol. In the case of two other tumor cells HepG2 and U87, the H_2O_2 released from cells were respectively ∼440 ± 24.3 and ∼375 ± 33.5 amol. It is obvious that there are more released H_2O_2 from three kinds of tumor than that of normal cell lines, as exhibited in Figure 8B. For instance, the amount of H_2O_2 by human cervical cancer cell HeLa was almost twice as much as that of the normal hepatic cells L02.

The production and distribution of H_2O_2 in cells irritated from AA can be attributed to the following views. The intracellular concentration of H_2O_2 is held at a stable level in favor of cellular activity and proliferation, the process of maintaining intracellular redox homeostasis is not only regulated by the catabolism but also affected by the H_2O_2 elimination.[2] When living cells were stimulated by external elements, the intracellular redox homeostasis was destroyed and excreted H_2O_2 induced by stress reaction. The diffusion of relevant H_2O_2 from high to low concentration regions was promoted by the method of free molecule diffusion readily crossing the lipid bilayer of membrane[35] or through the means similar to water which was facilitated by some channel proteins, such as aquaporins.[36,37] Then the extracellular and intracellular concentrations of H_2O_2 were regulated to remain at the same level, achieving the state of redox homeostasis again. What is more, it is considered that the tumor cells generated more H_2O_2 than normal cell lines, as a result of an elevation of ROS production capacity in abnormal growth of the tumor.[5] Therefore, the detection of the flux of H_2O_2 is meaningful for evaluation of living cell oxidative stress and has possibility in the application of investigation of oxidative stress capability distinctions in different living cells. It is also of certain significance for exploration of the environment in tumor cells and the therapy of cancer.

4. CONCLUSIONS

In summary, we have reported a nonenzymatic H_2O_2 sensor constructed on the basis of hybrid nanoelectrochemical catalysts of RGO/Au/Fe$_3$O$_4$/Pt nanocomposites, which were obtained through electrochemical deposition by a high amount of Pt nanoparticles. The robust nonenzymatic hybrid nanocatalysts RGO/Au/Fe$_3$O$_4$/Pt-modified GCE possess much better electrochemical catalysis properties and higher sensitivity for the measurement of H_2O_2 than that of one elemental modification of GCE (i.e., a relevant GCE electrode decorated by single nanomaterial alone). The results demonstrate that the nonenzymatic hybrid nanocatalysts RGO/Au/Fe$_3$O$_4$/Pt-based biosensor display high selectivity and sensitivity for oxidative stress such as H_2O_2 release, with relatively low overpotential of 0 V, low detection limit of ∼0.1 μM, large linear range from 0.5 μM to 11.5 mM, and outstanding reproducibility. This robust nonenzymatic biosensor has shown great potential applications in the determination of H_2O_2 released from the living cells including cancer cells, which is significant in the development of ultrasensitive nonenzyme biosensors for clinical diagnostics to rapidly assess oxidative stress of different kinds of diseased cells.

■ ASSOCIATED CONTENT

Supporting Information

The Supporting Information is available free of charge on the ACS Publications website at DOI: 10.1021/acsami.5b04553.

XPS studies of relevant nanocomposites to characterize the valence states of main elements of relevant nanocomposites and figures for EDS results of RGO/AuFe$_3$O$_4$ and Pt NPs (PDF)

DOI: 10.1021/acsami.5b04553
ACS Appl. Mater. Interfaces 2015, 7, 18441−18449

AUTHOR INFORMATION

Corresponding Author

*E-mail: xuewang@seu.edu.cn. Tel.: +86-25-83792177.

Notes

The authors declare no competing financial interest.

ACKNOWLEDGMENTS

This work is supported by the National High Technology Research & Development Program of China (Grant 2015AA020502), the National Natural Science Foundation of China (Grants 81325011, 21327902, and 21175020), and the Major Science & Technology Project of Suzhou (Grant ZXY2012028).

REFERENCES

(1) Zhang, Y.; Wu, C.; Zhou, X.; Wu, X.; Yang, Y.; Wu, H.; Guo, S.; Zhang, J. Graphene Quantum Dots/Gold Electrode and its Application in Living Cell H_2O_2 Detection. *Nanoscale* **2013**, *5*, 1816−1819.

(2) Chang, H.; Wang, X.; Shiu, K.-K.; Zhu, Y.; Wang, J.; Li, Q.; Chen, B.; Jiang, H. Layer-by-layer Assembly of Graphene, Au and Poly(Toluidine Blue O) Films Sensor for Evaluation of Oxidative Stress of Tumor Cells Elicited by Hydrogen Peroxide. *Biosens. Bioelectron.* **2013**, *41*, 789−794.

(3) Sanford, A. L.; Morton, S. W.; Whitehouse, K. L.; Oara, H. M.; Lugo-Morales, L. Z.; Roberts, J. G.; Sombers, L. A. Voltammetric Detection of Hydrogen Peroxide at Carbon Fiber Microelectrodes. *Anal. Chem.* **2010**, *82*, 5205−5210.

(4) Zhang, Y.; Bai, X.; Wang, X.; Shiu, K.-K.; Zhu, Y.; Jiang, H. Highly Sensitive Graphene−Pt Nanocomposites Amperometric Biosensor and Its Application in Living Cell H_2O_2 Detection. *Anal. Chem.* **2014**, *86*, 9459−9465.

(5) Khodade, V. S.; Sharath Chandra, M.; Banerjee, A.; Lahiri, S.; Pulipeta, M.; Rangarajan, R.; Chakrapani, H. Bioreductively Activated Reactive Oxygen Species (ROS) Generators as MRSA Inhibitors. *ACS Med. Chem. Lett.* **2014**, *5*, 777−781.

(6) Sahu, T.; Bisht, S. S.; Das, K. R.; Kerkar, S. Nanoceria: Synthesis and Biomedical Applications. *Curr. Nanosci.* **2013**, *9*, 588−593.

(7) Borgmann, S. Electrochemical Quantification of Reactive Oxygen and Nitrogen: Challenges and Opportunities. *Anal. Bioanal. Chem.* **2009**, *394*, 95−105.

(8) Wen, F.; Dong, Y.; Feng, L.; Wang, S.; Zhang, S.; Zhang, X. Horseradish Peroxidase Functionalized Fluorescent Gold Nanoclusters for Hydrogen Peroxide Sensing. *Anal. Chem.* **2011**, *83*, 1193−1196.

(9) Wang, K.; Liu, Q.; Wu, X. Y.; Guan, Q.-M.; Li, H. N. Graphene Enhanced Electrochemiluminescence of CdS Nanocrystal for H_2O_2 Sensing. *Talanta* **2010**, *82*, 372−376.

(10) Gimeno, P.; Bousquet, C.; Lassu, N.; Maggio, A. F.; Civade, C.; Brenier, C.; Lempereur, L. High-performance Liquid Chromatography Method for The Determination of Hydrogen Peroxide Present or Released in Teeth Bleaching Kits and Hair Cosmetic Products. *J. Pharm. Biomed. Anal.* **2015**, *107*, 386−393.

(11) Hua, M. Y.; Chen, H. C.; Chuang, C. K.; Tsai, R. Y.; Jeng, J. L.; Yang, H. W.; Chern, Y. T. The Intrinsic Redox Reactions of Polyamic Acid Derivatives and their Application in Hydrogen Peroxide Sensor. *Biomaterials* **2011**, *32*, 4885−4895.

(12) Li, J.; Li, Y.; Zhang, Y.; Wei, G. Highly Sensitive Molecularly Imprinted Electrochemical Sensor Based on the Double Amplification by an Inorganic Prussian Blue Catalytic Polymer and the Enzymatic Effect of Glucose Oxidase. *Anal. Chem.* **2012**, *84*, 1888−1893.

(13) Chakraborty, S.; Raj, C. R. Pt Nanoparticle-based Highly Sensitive Platform for the Enzyme-free Amperometric Sensing of H_2O_2. *Biosens. Bioelectron.* **2009**, *24*, 3264−3268.

(14) Liu, X.; Feng, H.; Zhang, J.; Zhao, R.; Liu, X.; Wong, D. K. Hydrogen Peroxide Detection at a Horseradish Peroxidase Biosensor with a Au Nanoparticle−dotted Titanate Nanotube| Hydrophobic Ionic Liquid Scaffold. *Biosens. Bioelectron.* **2012**, *32*, 188−194.

(15) Wang, H.; Lang, Q.; Li, L.; Liang, B.; Tang, X.; Kong, L.; Mascini, M.; Liu, A. Yeast Surface Displaying Glucose Oxidase as Whole-cell Biocatalyst: Construction, Characterization, and its Electrochemical Glucose Sensing Application. *Anal. Chem.* **2013**, *85*, 6107−6112.

(16) Baj-Rossi, C.; Jost, T. R.; Cavallini, A.; Grassi, F.; De Micheli, G.; Carrara, S. Continuous Monitoring of Naproxen by a Cytochrome P450-based Electrochemical Sensor. *Biosens. Bioelectron.* **2014**, *53*, 283−287.

(17) Hu, J.; Yu, Y.; Guo, H.; Chen, Z.; Li, A.; Feng, X.; Xi, B.; Hu, G. Sol−gel Hydrothermal Synthesis and Enhanced Biosensing Properties of Nanoplated Lanthanum-substituted Bismuth Titanate microspheres. *J. Mater. Chem.* **2011**, *21*, 5352−5359.

(18) Jiaojiao, J.; Yangyang, G.; Gangying, Z.; Yanping, C.; Wei, L.; Guohua, H. D-Glucose, D-Galactose, and D-Lactose Non-enzyme Quantitative and Qualitative Analysis Method Based on Cu Foam Electrode. *Food Chem.* **2015**, *175*, 485−493.

(19) Liu, Z.; Zhao, B.; Shi, Y.; Guo, C.; Yang, H.; Li, Z. Novel Nonenzymatic Hydrogen Peroxide Sensor Based on Iron Oxide−silver Hybrid Submicrospheres. *Talanta* **2010**, *81*, 1650−1654.

(20) Yan, X.; Chen, J.; Yang, J.; Xue, Q.; Miele, P. Fabrication of Free-standing, Electrochemically Active, and Biocompatible Graphene Oxide − Polyaniline and Graphene− Polyaniline Hybrid papers. *ACS Appl. Mater. Interfaces* **2010**, *2*, 2521−2529.

(21) Wang, Y.; Li, Y.; Tang, L.; Lu, J.; Li, J. Application of Graphene-modified Electrode for Selective Detection of Dopamine. *Electrochem. Commun.* **2009**, *11*, 889−892.

(22) Bai, X.; Chen, G.; Shiu, K. K. Electrochemical Biosensor Based on Reduced Graphene Oxide Modified Electrode with Prussian Blue and Poly (Toluidine Blue O) Coating. *Electrochim. Acta* **2013**, *89*, 454−460.

(23) Gong, H.; Sun, M.; Fan, R.; Qian, L. One-step Preparation of a Composite Consisting of Graphene Oxide, Prussian Blue and Chitosan for Electrochemical Sensing of Hydrogen Peroxide. *Microchim. Acta* **2013**, *180*, 295−301.

(24) Zhou, M.; Zhai, Y.; Dong, S. Electrochemical Sensing and Biosensing Platform Based on Chemically Reduced Graphene Oxide. *Anal. Chem.* **2009**, *81*, 5603−5613.

(25) Wu, P.; Cai, Z.; Gao, Y.; Zhang, H.; Cai, C. Enhancing the Electrochemical Reduction of Hydrogen Peroxide Based on Nitrogen-doped Graphene for Measurement of its Releasing Process from Living Cells. *Chem. Commun.* **2011**, *47*, 11327−11329.

(26) Pagliari, F.; Mandoli, C.; Forte, G.; Magnani, E.; Pagliari, S.; Nardone, G.; Licoccia, S.; Minieri, M.; Di Nardo, P.; Traversa, E. Cerium Oxide Nanoparticles Protect Cardiac Progenitor Cells from Oxidative Stress. *ACS Nano* **2012**, *6*, 3767−3775.

(27) Pumera, M. Graphene-based Nanomaterials and Their Electrochemistry. *Chem. Soc. Rev.* **2010**, *39*, 4146−4157.

(28) Haruta, M. Catalysis of Gold Nanoparticles Deposited on Metal Oxides. *CATTECH* **2002**, *6*, 102−115.

(29) Chen, M.; Goodman, D. The Structure of Catalytically Active Gold on Titania. *Science* **2004**, *306*, 252−255.

(30) Liu, Z.-P.; Gong, X.-Q.; Kohanoff, J.; Sanchez, C.; Hu, P. Catalytic Role of Metal Oxides in Gold-Based Catalysts: A First Principles Study of CO Oxidation on TiO_2 Supported Au. *Phys. Rev. Lett.* **2003**, *91*, 266102.

(31) Lee, Y.; Garcia, M. A.; Frey Huls, N. A.; Sun, S. Synthetic Tuning of the Catalytic Properties of Au-Fe_3O_4 Nanoparticles. *Angew. Chem.* **2010**, *122*, 1293−1296.

(32) Molina, L.; Hammer, B. Active Role of Oxide Support during CO Oxidation at Au/MgO. *Phys. Rev. Lett.* **2003**, *90*, 206102.

(33) Xu, F.; Sun, Y.; Zhang, Y.; Shi, Y.; Wen, Z.; Li, Z. Graphene−Pt Nanocomposite for Nonenzymatic Detection of Hydrogen Peroxide with Enhanced Sensitivity. *Electrochem. Commun.* **2011**, *13*, 1131−1134.

(34) Chu, X.; Duan, D.; Shen, G.; Yu, R. Amperometric Glucose Biosensor Based on Electrodeposition of Platinum Nanoparticles onto Covalently Immobilized Carbon Nanotube Electrode. *Talanta* **2007**, *71*, 2040−2047.

DOI: 10.1021/acsami.5b04553
ACS Appl. Mater. Interfaces 2015, 7, 18441−18449

(35) Bienert, G. P.; Schjoerring, J. K.; Jahn, T. P. Membrane Transport of Hydrogen Peroxide. *Biochim. Biophys. Acta, Biomembr.* **2006**, *1758*, 994−1003.
(36) Bienert, G. P.; Møller, A. L.; Kristiansen, K. A.; Schulz, A.; Møller, I. M.; Schjoerring, J. K.; Jahn, T. P. Specific Aquaporins Facilitate the Diffusion of Hydrogen Peroxide Across Membranes. *J. Biol. Chem.* **2007**, *282*, 1183−1192.
(37) Halliwell, B.; Clement, M. V.; Ramalingam, J.; Long, L. H. Hydrogen Peroxide. Ubiquitous in Cell Culture and in Vivo? *IUBMB Life* **2000**, *50*, 251−257.

DOI: 10.1021/acsami.5b04553
ACS Appl. Mater. Interfaces 2015, 7, 18441−18449